# Investigating the Thermal Profile of a Marine Vessel Engine Room through Simulation with Field Measurements

Will Newton[1*], Mel Lewis[2], Dave Carswell, Nicholas P. Lavery, Ben Evans, David Bould, Johann Sienz

[1]ASTUTE, Digital Technium, Swansea University, SA2 8PP, UK
w.newton@swansea.ac.uk
[2] Mustang Marine, The Dockyard, Pembroke Dock, Pembrokeshire, SA72 6TE, UK

*Corresponding author. Tel.: +44(0)1792606876; E-mail address: w.newton@swansea.ac.uk

**Abstract**
This paper assesses the use of computational fluid dynamics (CFD) to model the ventilation of a working marine vessel, its performance in extreme climates, and potential improvements to the ventilation system which could lead to increased efficiencies of the engine and generator set.

Comparisons between data gathered on the marine vessel and the computational model show good agreement, with an average discrepancy in temperature of 0.4 %. The model showed that the current ventilation system was inadequate for the use of the marine vessel in Arctic waters. In contrast, the model showed the vessel was suited for tropical waters, and that the boat complied with British Standards for ventilation.

Directing the flow within the engine room was found to improve the overall cooling of the room, and reduce the range of temperatures to improve thermal comfort. Directing the flow has shown reduced intake temperatures of the engine and generator set, improving efficiencies by 0.5 % and 0.57 % respectively. This paper demonstrates that the use of CFD to model marine vessel engine rooms can be used in retrospective design of ventilation systems, furthermore, it can be a tool utilised in the design stages for optimised engine rooms ventilation systems.

*Key words: Thermal modelling, Engine room, Forced ventilation, CFD*

## 1. Introduction

Engine rooms in marine vessels require ventilation for a number of purposes due to the essential components which lie within, Diesel engines used for propulsion and generating electricity are exposed to varying climatic conditions, from the cold ambient conditions in the Arctic to the warmth of the tropics. These engines must continue to work within all environments.

The ventilation of the engine rooms is vitally important and has a range of purposes; providing the air for combustion to the engines, providing the engines with cool air to extract unwanted heat, maintaining the temperature within an adequate range so personnel can work in the engine room [1], and electrical components do not over heat.

Whilst large boat and engine manufacturers may have advanced engineering facilities with longstanding experience in this area, there is very little published research directly relating the use of CFD to the ventilation of marine engine rooms, apart from commercial engineering companies which may provide case studies such as [2] which is very closely linked to the work presented in this paper.

Engine manufacturers often provide advice on the amount of air required for combustion, but do not always advise on the flow of air required to account for the cooling of the engine. Certain manufacturers provide some assistance on the

overall engine room ventilation, such as CAT [3] and Cummins [4]. This required air flow through the engine room is usually calculated using average ambient conditions, and does not take into account extreme climatic conditions that could be associated. Within the UK, British Standard BS EN ISO 8861:1998 [1] states the temperature must not exceed an increase of more than 12.5 K from engine room inlet to the personnel entrance of the engine room when the ambient air temperature is 308.0 K. The standard also specifies the minimum amount of air through an engine room as a function of the air required for combustions, and the heat output from the engine(s).

Boat manufacturers often consider the engine room as a low priority, preferring to meet clients' requests for more space above the engine room, which means many vital components to the boat are confined to a small space, and the ventilation system is sized to meet the aforementioned engine manufacturer's guidelines. This can lead to awkward spaces which are poorly ventilated, causing low efficiencies in heat transfer, often compensated with an excessively large ventilation system.

Computational Fluid Dynamics (CFD) is increasingly being used within all aspects of industry, from automotive to civil engineering. As the cost of computing has decreased, the use of CFD has become more affordable, especially when considering the costs of experimentation. Whilst there is very little published in terms of ventilation for marine vessel engine rooms, there is a large amount of published work in the form of ventilating occupied spaces, such as buildings [5], [6], aeroplane cabins [7] [8] and automobiles [9].

Ramos *et al* [10] used CFD to model the ventilation of underground transformer substations, and validated with experimental results. The simulations allowed a thermal analysis within the substations which could not be done easily through experiments. The results of the CFD model will allow the authors to develop further tools to optimise the designs.

Rohdin *et al* [5] investigated the ventilation system of an industrial building. A CFD model was used to investigate various turbulence models which were compared to experimental data. The Re-Normalisation Group turbulence model [11], found in Fluent [12], was deemed the best suited to the experimental data. The validated model was used to compare between mixing and displacement ventilation supply systems. Rohdin *et al* concluded displacement supply was superior.

The methodology used by Ramos *et al* [10] and Rohdin *et al* [5] was similar to that of the work presented in this paper, using experimental data in conjunction with CFD to conduct a thermal analysis, however, the application is different in each case. Although the same methodology has been used to validate a computer model, the eventual use of the model is where the research differs. In the present work, engine efficiencies are investigated as a function of intake temperatures.

The purpose of the work presented was to devise a strategy to accurately model a marine vessel engine room and validate against field measurements. A baseline model was used to assess the impact of computational parameters, such as grid refinement and turbulence models, which makes use of the room layout and boundary conditions as measured in the experiments.

The model was then used for an investigation into the overall thermal profiles for extreme climates. The main focus of the work was to conduct an investigation into the use of ducted inlets and outlets to direct the flow around the room for improved efficiencies of the engine and generator set (Genset) for sustainability. Whilst most publications focus on the ventilation efficiency due to removal of contaminants, this was not considered, rather, the performance indicators were the average

temperature working conditions for personnel, but more importantly, the efficiencies of engines due to the intake temperatures.

## 2. Description of the engine room

The boat considered is a catamaran type vessel 18 m long and has an engine room within each hull. Each engine room has dimensions of $x$ = 1.9 m, $y$ = 4.9 m and $z$ = 1.8 m. Within each room a diesel propulsion engine, a diesel electricity generator (Genset) and many electrical components, such as wiring and control boxes, are present, which can be seen in Fig. 1. The engine room of interest is within the starboard hull, as the Genset is air cooled within this engine room. The propulsion engine is a turbocharged v6 diesel engine producing a power of 261.0 kW at full loading, whilst the Genset utilises a naturally aspirated diesel engine producing a power of 26.7 kW.


**Fig. 1.** Photograph of engine room showing the engine (green) and Genset (red).

Air is delivered to the front starboard side of the room by means of an axial fan which is situated externally above, whilst the outlet is positioned toward the rear of the room on the same side, and is left open to atmospheric conditions. Both the inlet and outlet have filters to prevent any particulates or spray entering the room. The locations of the inlet and outlet can be seen, along with the engine and Genset, in a simplified CAD model in Fig. 2. The engine has a single intake for air for combustion, the main cooling for the engine is conducted through a dual heat exchanger using sea water as the final coolant. The exhaust is taken directly out of the room through insulated pipes. The Genset has a single inlet for combustion air, however, uses a radiator for cooling, where air is drawn over the Genset by a fan, and hot air exhausted into the room, the combustion exhaust gases are also taken out of the room by exhaust pipes.

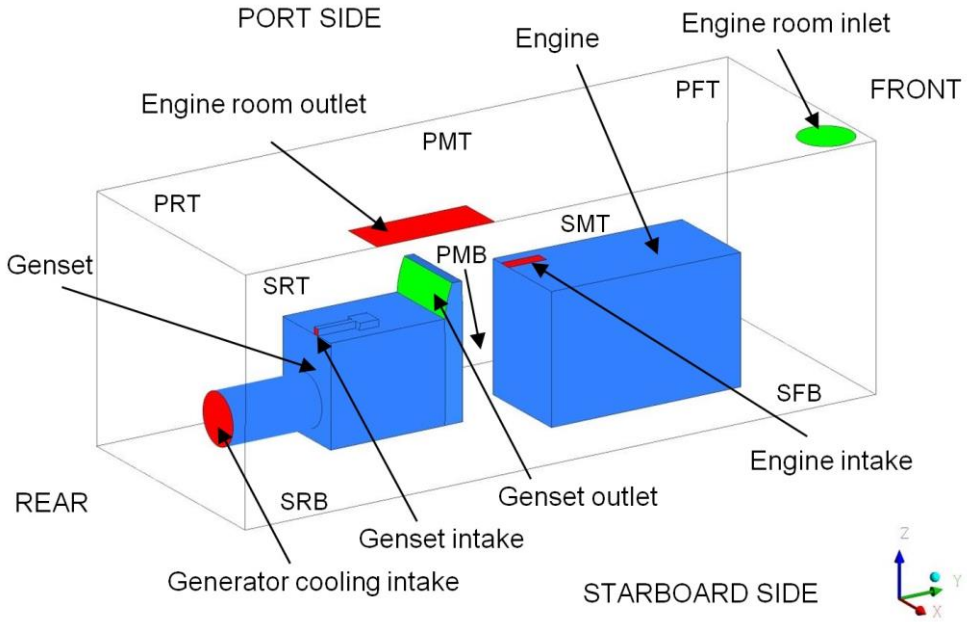


**Fig. 2.** Geometry of engine room. (Three letter acronyms represent data point location, e.g. SFB = Starboard Front Bottom. Colour of green represents inlets to the computational domain, red represent outlet of the computational domain).

## 3. Experimental

Experimental data was acquired as in-field measurements whilst the boat was going through commissioning during which a number of speed trials were conducted. A full speed trial was of interest, where the engine and Genset were on full power. Data was recorded for flow rates, temperature, pressure and humidity. Flow rates and temperatures were logged by manufacturer-calibrated wind vane anemometers for flow into the engine room, the engine air intake, the Genset air intake and Genset cooling outlet. The anemometers logged data at 1 second intervals, and had an error of 2 % + 0.2 m/s. Additional temperature data was recorded by Pico loggers using thermocouples at a number of locations around the room for air flow, and surface mounted thermocouples on the engine and Genset. The locations of the thermocouples can be seen in Fig. 2 indicated by three letter acronyms, *e.g.* SFB = Starboard Front Bottom, and in Fig. 3 where the regions have been split into the port and starboard sides, front middle and rear, and the top and bottom, whilst two pictures of the thermocouple placement for port rear bottom and top are shown in Fig. 4.

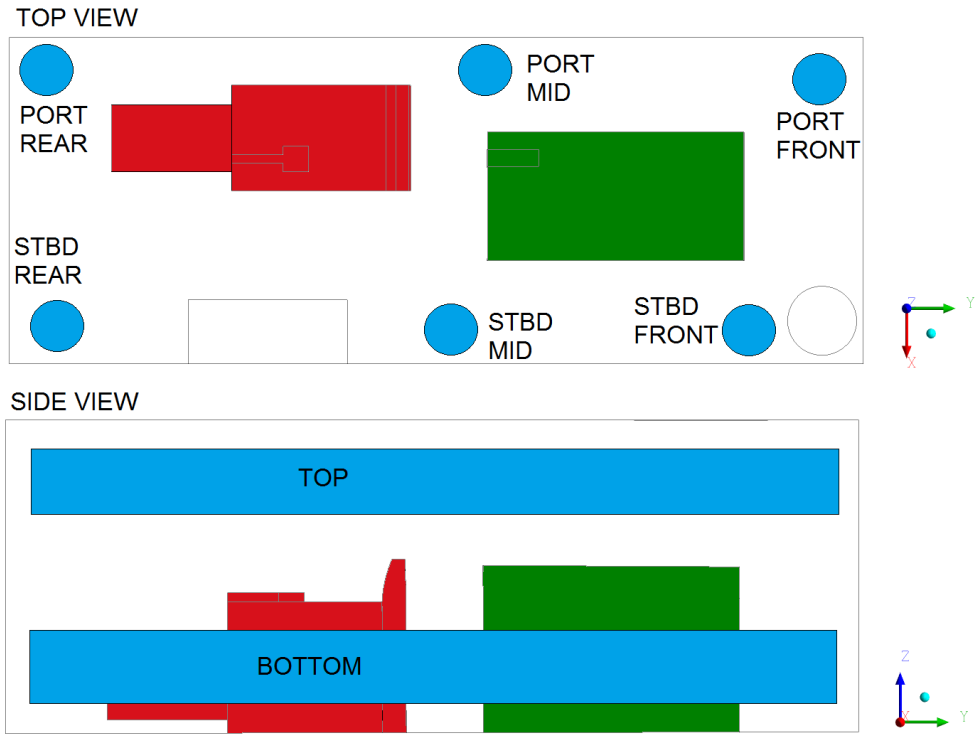


**Fig. 3.** Top and side view of engine room to show locations of thermocouples.

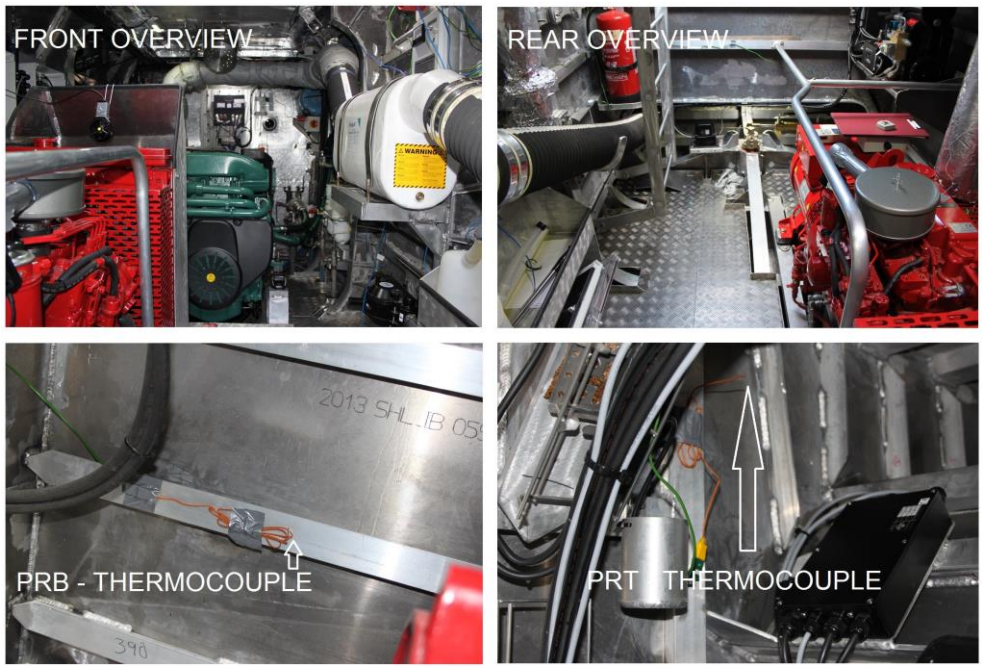


**Fig. 4.** Overview of engine room and thermocouple placement.

The data was recorded from the thermocouples at 1 second intervals and had an associated error of +/- 2.2 K. A thermal imaging camera was used to capture surface temperatures of the engine and Genset which was validated with the surface mounted thermocouple data. The trials lasted for 4 hours, with the full speed trial lasting 1 hour. This gave the engine room sufficient time for temperature and flow to reach a steady state. The surface temperatures and flow conditions were used as boundary conditions for the computational model, whilst the temperature profile of the room was used for validation of the computational model.

## 4. Computational model

### *4.1. Governing equations*

The conservation of mass, momentum and energy laws govern the flow of air and temperature distribution within the engine room. The flows were assumed to be steady state, as the experimental trials were run on this basis with no time dependent conditions. The flow was considered to be three-dimensional, incompressible and turbulent, and the density based on the incompressible ideal gas law within Fluent, with a Reynolds number of 369,805 and a Prandtl number of 0.707 for the baseline model. Radiation heat transfer was not included because at the relatively low temperatures of the solution, the effect of radiation heat transfer to the flow of air would be minimal. Following from the assumptions outlined, the flow can be described by the time averaged, discretised equations for continuity, momentum and energy

$$\frac{\partial(\rho u_i)}{\partial x_i} = 0 \quad \textbf{(1)}$$

$$u_j \frac{\partial u_i}{\partial x_j} = -\frac{1}{\rho}\frac{\partial p}{\partial x_i} + \frac{1}{\rho}\frac{\partial \tau_{ij}}{\partial x_j} \quad \textbf{(2)}$$

$$u_j \frac{\partial E}{\partial x_j} + \frac{1}{\rho}\frac{\partial p}{\partial x_i}\left(k\frac{\partial T}{\partial x_i}\right) + \frac{1}{\rho}\frac{\partial(u_j p)}{\partial x_j} - \frac{1}{\rho}\frac{\partial(\tau_{ij}u_j)}{\partial x_i} = 0 \quad \textbf{(3)}$$

where $\rho$ is density, $u$ is velocity, $p$ is pressure, $\tau$ is deviatoric stress, $E$ is total energy, $k$ is thermal conductivity, $T$ is temperature and subscripts $i$ and $j$ represent direction a 3D Cartesian coordinate system and the summation convention is assumed.

The nature of the flow within the room was complex, with a jet like inlet condition impacting on the floor of the room, before dispersing throughout the room, with two large bluff bodies, causing a separation and a swirling natured flow. Due to the nature of the flow, the Realizable $k-\varepsilon$ model [13] was deemed most appropriate [14]. A study into the other turbulence models within FLUENT confirmed the RKE model was the most suitable.

The RKE model is a modified version of the well documented $k-\varepsilon$ model due to a modified transport equation for $\varepsilon$ and a different formulation for the turbulent viscosity. The RKE model was developed to improve the accuracy of modelling the spreading rate of jets and flows involving separation and recirculation. The turbulent kinetic energy, $k$, and the rate of dissipation, $\varepsilon$, are obtained from the transport equations

$$\frac{\partial}{\partial t}(\rho k) + \frac{\partial}{\partial x_i}(\rho k u_i) = \frac{\partial}{\partial x_j}\left[\left(\mu + \frac{\mu_t}{\sigma_k}\right)\frac{\partial k}{\partial x_j}\right] + G_k + G_b - \rho\varepsilon \quad \textbf{(4)}$$

$$\frac{\partial}{\partial t}(\rho \varepsilon) + \frac{\partial}{\partial x_i}(\rho \varepsilon u_i) = \frac{\partial}{\partial x_j}\left[\left(\mu + \frac{\mu_t}{\sigma_\varepsilon}\right)\frac{\partial \varepsilon}{\partial x_j}\right] + \rho C_1 S_\varepsilon - \rho C_2 \frac{\varepsilon^2}{k + \sqrt{\nu\varepsilon}} + C_{1\varepsilon}\frac{\varepsilon}{k}C_{3\varepsilon}G_b \quad \textbf{(5)}$$

where $\mu_t$ is the turbulent kinetic viscosity, $G_k$ and $G_b$ are the generation of turbulence kinetic energy due to the mean velocity and due to buoyancy respectively, $\sigma_\varepsilon$ and $\sigma_k$ are the turbulent Prandtl numbers and $C_{1\varepsilon}$ , $C_{2\varepsilon}$ and $C_{3\varepsilon}$ are constants.

*4.3. Grid*

For the baseline model, five grids were used ranging from 1,200,000 to 10,000,000 hexahedral elements were constructed using ICEM [15]. A structured meshing technique was used, clustering the elements close to the surfaces where temperature boundary conditions existed and greater gradients are expected. Steady state convergence was only achieved across all grids for one turbulence model, the RKE turbulence model. Considering computational resources, a mesh with a grid size of 1,500,000 elements was used, the surface mesh shown in Fig. 5 and Fig. 6. Areas shaded green are inlets into the computation domain, whilst red are outlets from the domain.

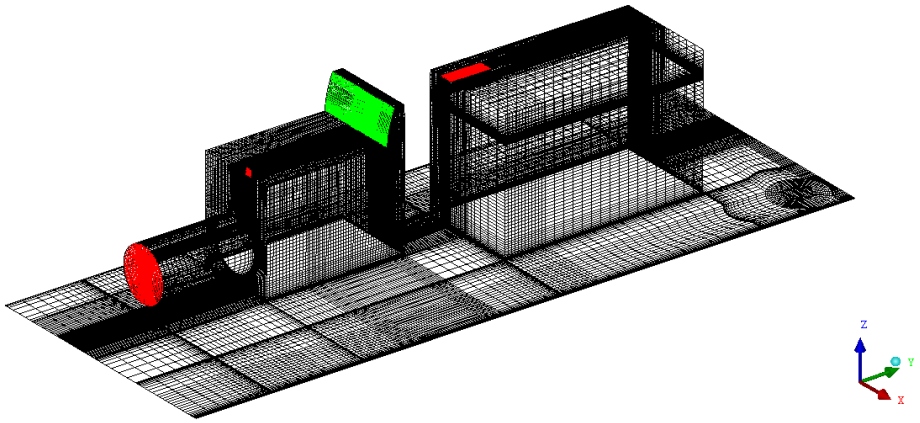


**Fig. 5.** Computational grid used for study, perspective view of surface mesh for components.

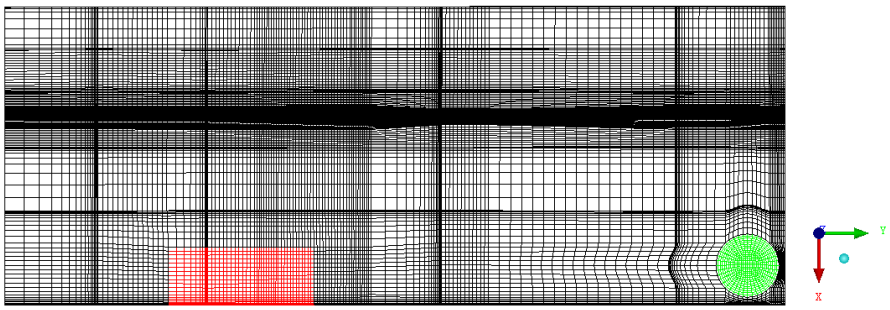


**Fig. 6.** Computational grid used for study, top view of surface mesh including inlet and outlet.

For the second part of the study, flow was directed around the room by means of ducted inlets/outlets. A second model was generated with the required additional geometry. Again, 5 levels of grid resolution were used in the same manner as the baseline model to show grid convergence. The two lowest grid sizes on the second model did not produce acceptable solutions due to non-agreement in solutions, however, the solutions were in agreement for the remaining three grid sizes upwards from 3,200,000 elements. A grid size of 3,200,000 elements was used.

*4.4. Numerical accuracy*

FLUENT v14.0 [12] was used to simulate the air flow and heat transfer across the engine room. The governing equations were discretised with a second order upwind scheme, using the SIMPLE algorithm to couple the momentum and pressure equations [16]. The solution was considered converged when the

normalised residuals for continuity, momentum and turbulence reached $10^{-3}$ and energy $10^{-6}$ respectively.

## 5. Case studies and boundary conditions

A range of cases were studied, firstly to compare turbulence models and grid resolution to the experimental data. The appropriate model was then used to study the effects of varying the boundary conditions to simulate different extreme climates. Arctic conditions were simulated by varying the temperature of the incoming air, which was reduced to 258.0 K, and Tropical conditions were simulated by increasing the temperature of the incoming air to 308.0 K. Lastly, studies were conducted to evaluate the effect of ducting the inlet flow into the engine room to direct the flow onto the engine and Genset, and ducting the flow out of the Genset directly out of the room.

### *5.1. Baseline case and climatic study*

The boundary conditions for the baseline computational model were acquired from the experimental data. The flow velocity and temperature were recorded for each of the inlets and outlets to the room and engines. Surface temperatures of the engine and Genset were determined by using a thermal imaging camera used in conjunction with surface mounted thermocouples. The boundary conditions for the baseline case and the two cases for the climatic study can be seen in Table 1.

**Table 1.** Boundary conditions for climatic study cases.

| | | Case 1 Baseline | Case 2 Arctic | Case 3 Tropics |
|---|---|---|---|---|
| Engine room inlet | velocity (m/s) | 14.5 | 14.5 | 14.5 |
| | temperature (K) | 291.0 | 258.0 | 308.0 |
| | relative humidity (%) | 50 | 80 | 68 |
| Engine | surface temperature (K) | 353.0 | 353.0 | 353.0 |
| | intake velocity (m/s) | 4.0 | 4.0 | 4.0 |
| Genset | surface temperature (K) | 333.0 | 333.0 | 333.0 |
| | intake velocity (m/s) | 16.0 | 16.0 | 16.0 |
| | outlet velocity (m/s) | 4.0 | 4.0 | 4.0 |
| | outlet temperature (K) | 323.0 | 323.0 | 323.0 |
| Generator cooling | velocity (m/s) | 3.0 | 3.0 | 3.0 |
| Engine room outlet | gauge pressure (Pa) | 0 | 0 | 0 |

### *5.2. Ducted inlet study*

For the ducted inlet studies, additional inlets were introduced to represent ducted flow into the room. Two inlets were added, both at the top of the front wall as these could be introduced into the real engine room relatively easily. The inlet named mid_E was aligned with the engine along the *x*-axis, whilst the inlet named mid_G was aligned with the Genset along the *x*-axis, the additional inlets can be seen in Fig. 7.

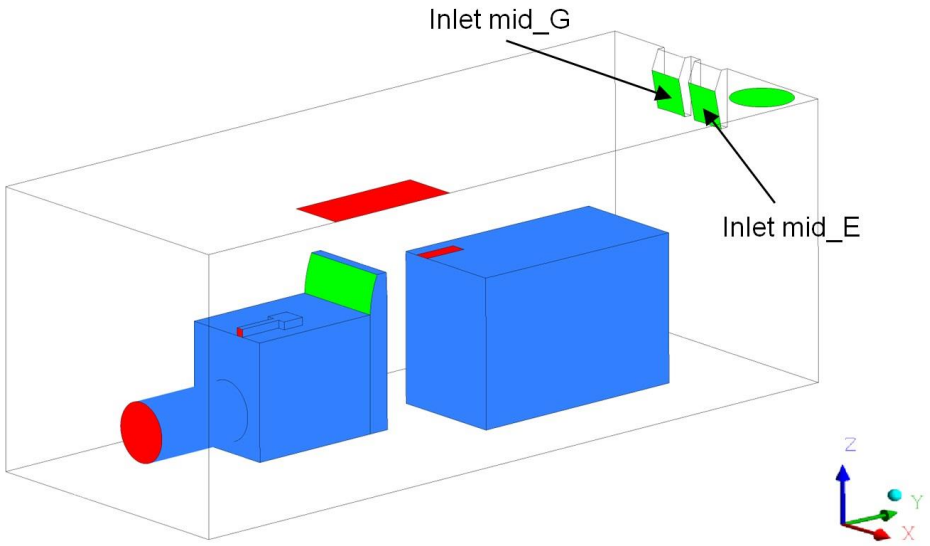


**Fig. 7.** Additional inlets to represent ducted flow into the engine room.

The overall mass flow into the engine room was split equally across each of the inlets for each the simulations, and can be seen in Table 2. All other boundary conditions remained the same as the baseline case, Case 1.

**Table 2.** Engine room inlet velocities for ducted inlet study.

| Name | Inlet (m/s) | Inlet mid_E (m/s) | Inlet mid_G (m/s) |
|---|---|---|---|
| Case 4 | 0 | 14.5 | 14.5 |
| Case 5 | 7.5 | 14.5 | 0 |
| Case 6 | 7.5 | 0 | 14.5 |
| Case 7 | 7.5 | 7.5 | 7.5 |

### *5.3. Ducted Genset outlet study*

For the ducted Genset outlet study, the flow out of the Genset was turned off, thus representing flow being ducted directly out of the room. All ducted simulations were repeated with the Genset outlet boundary condition turned off, with the remainder of the boundary conditions remaining the same. For clarification, the studied cases are shown in Table 3.

**Table 3.** Engine room inlet velocities for ducted Genset outlet study.

| Name | Inlet (m/s) | Inlet mid_E (m/s) | Inlet mid_G (m/s) |
|---|---|---|---|
| Case 8 | 14.5 | 0 | 0 |
| Case 9 | 0 | 14.5 | 14.5 |
| Case 10 | 7.5 | 14.5 | 0 |
| Case 11 | 7.5 | 0 | 14.5 |
| Case 12 | 7.5 | 7.5 | 7.5 |

## 6. Measurement of performance

To evaluate the performance of the boat within waters at the extreme ends of the climatic conditions, two performance indicators were used. The first was the overall

thermal profile which can be used to assess the thermal comfort for working personnel. The British Standard [1] for engine room ventilation design requirements was used to assess this. The second was the heat removal effectiveness, which is calculated from [17]:

$$\varepsilon_T = \frac{T_o - T_i}{T_m - T_i} \quad \textbf{(6)}$$

where $T$ is temperature, and subscripts $i$, $o$ and $m$ represent the temperature conditions at the inlet, at the outlet and the mean temperature for the occupied zone, which in the case of the engine room is the entire flow field.

The main focus of the paper was to assess whether an improvement of efficiencies for the engine and Genset could be achieved through ducting the air flow, as higher efficiencies can be achieved if intake temperatures are reduced. The British Standard [18] for power correction of engines has been used to show these effects. The corrected power is calculated from known test conditions to differing conditions using the power correction, $\alpha_c$

$$\alpha_c = (f_a)^{f_m} \quad \textbf{(7)}$$

where $f_a$ is the atmospheric factor and $f_m$ is the engine factor.

For turbo charged diesel engines with charge air cooling, $f_a$ is calculated by

$$f_a = \left(\frac{p_r - \Phi_r p_{sr}}{p_y - \Phi_y p_{sy}}\right)^{0.7} \left(\frac{T_y}{T_r}\right)^{0.7} \quad \textbf{(8)}$$

and for naturally aspirated diesel engines, $f_a$ is calculated by

$$f_a = \left(\frac{p_r - \Phi_r p_{sr}}{p_y - \Phi_y p_{sy}}\right) \left(\frac{T_y}{T_r}\right)^{0.7} \quad \textbf{(9)}$$

where $p$ is the ambient pressure, $\Phi$ is the relative humidity, $p_s$ is the ambient saturated water vapour pressure, $T$ is the ambient air temperature, and subscripts r and y are reference site and test site respectively.

The engine factor is calculated by

$$f_m = 0.036 \left(\frac{q}{r_r}\right) - 1.14 \quad \textbf{(10)}$$

where $r_r$ is the ratio between static pressure at the compressor inlet and outlet at standard reference conditions, and equal to 1 for naturally aspirated engines, and $q$ is calculated from

$$q = \frac{Z \times \dot{q}}{V \times n} \quad \textbf{(11)}$$

where $Z$ is a constant which is equal to 120,000 for turbo charged engines, and 60,000 for naturally aspirated engines, $\dot{q}$ is the mass flow of the fuel, $V$ is the engine displacement, and $n$ is the speed of the engine, and the equation is only valid over the range

$$37.2 \leq q_c \leq 65 \quad \textbf{(12)}$$

The corrected power can then be found from

$$P_r = \alpha_c \times P_y \quad \textbf{(13)}$$

where $P$ is the brake power.

## 7. Results

The results are split into four sections; the first is the comparison between the experimental and the simulated data, the second is the varying ambient conditions and the third and fourth are for the ducted studies.

### *7.1. Comparison of experimental and simulated data*

The temperature data for the fluid flow that was logged during the experiment and extracted from the computational model are shown together for comparison in Fig. 8.

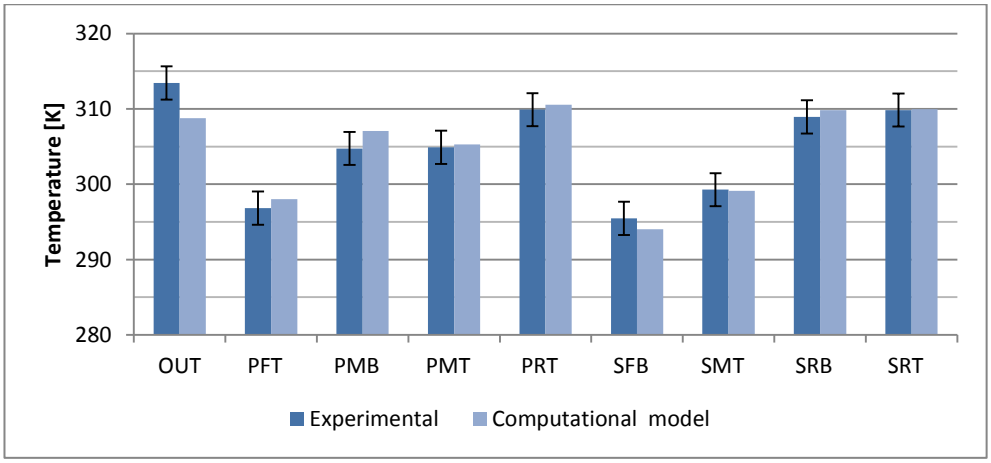


**Fig. 8.** Experimental and computational model comparison (error bars – manufacturers stated accuracy).

The computational model results show excellent agreement with experimental data. The average discrepancy between the simulated and experimental data sets was 0.4 % with a maximal difference of 1.45 % at the data point location “OUT”, which is the outlet of the engine room. For the experimentation the thermocouple was located close to an exhaust pipe, which was lagged, but means this could be a stagnant flow point where temperature can rise. This geometric obstacle was omitted from the simplified computational model to allow a structured grid to be generated. A maximal difference of 1.45 % was deemed acceptable. For the remaining points, apart from SFB, the model tends to over predict the temperature, albeit, by a small margin and within the errors associated with the experimentation. Therefore, it was concluded the overall results of the computational model describe the physics associated within the engine room with sufficient accuracy [19].

### *7.2. Ambient conditions case*

To compare the results for the varying ambient conditions cases, the same data point locations were used as previously, but with the inclusion of the intake temperatures of the engine and Genset, shown in Fig. 9. A contour plot of the three simulation results is shown in Fig. 10, where an *yz* plane has been created at *x* = 0.705 m, to show the full extent of the results.

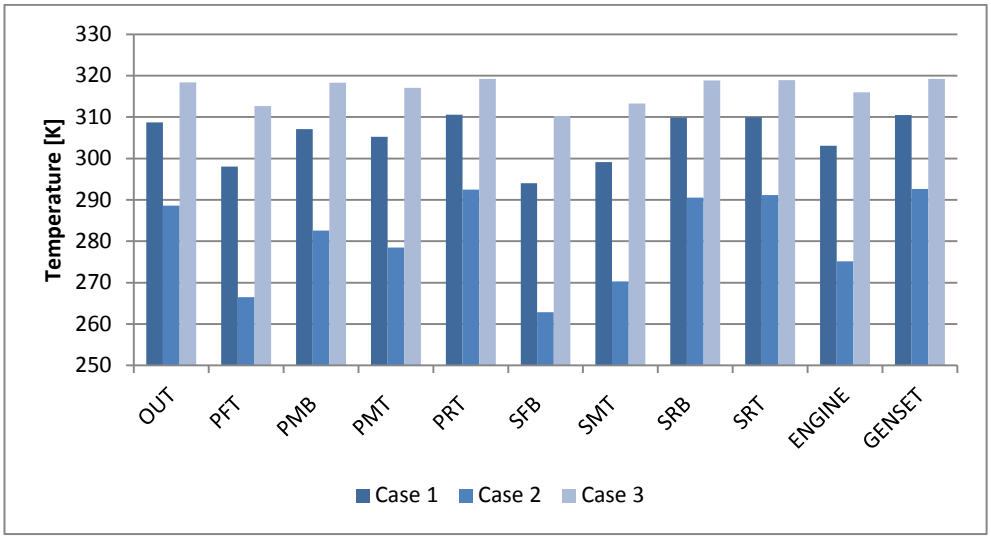


**Fig. 9.** Temperature at data locations for varying ambient conditions. Case 1 – baseline, Case 2 – Arctic, Case 3 – Tropics.

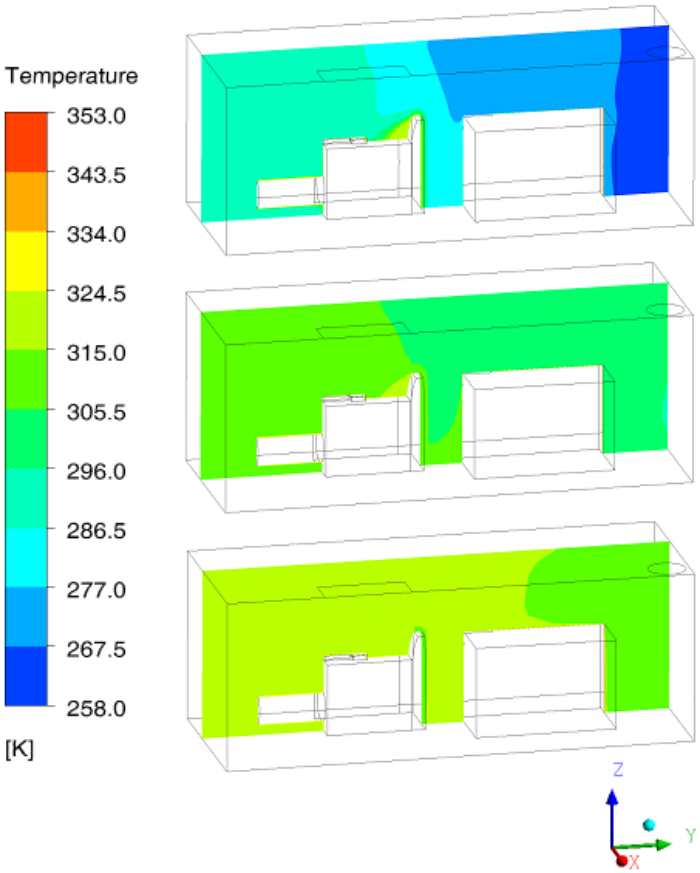


**Fig. 10.** Temperature profiles of engine room (*yz* plane at *x* = 0.705 m); top to bottom: Case 2 (Arctic), Case 1 (baseline), Case 3 (Tropics).

For Case 1, the range within the room is quite large, as the inlet temperature is 291.0 K and the Genset outlet temperature is 333.0 K, but at the data points, this range is reduced, with OUT being the hottest data point at 308.8 K. The profile can be split into three sections; the front of the room is the cold section, in the region of 291.0 K, due to the immediate effect of the cool air coming in from the fan, the middle section is slightly warmer, from 299.1 – 309.6 K, due to the air being heated

as it passes the main engine, and the rear of the room as hot as 322.0 K, due to a combination of the air being continually heated by the engine and Genset as it travels from the front to the back, plus the addition of hot air being exhausted from the Genset. In terms of thermal comfort, this poses a large temperature range in a small vicinity, which could be considered uncomfortable for personnel [1]. The effectiveness of heat removal for the baseline case was 0.98.

The temperature distribution of the air flow is much larger for the Arctic conditions, Case 2, from the incoming air at 258.0 K to the hot spot of the Genset outlet temperature at 333.0 K. The same temperature pattern is observed as Case 1, in terms of the front, middle and rear, however, the highest temperature is found at PRT. Personnel would find it difficult working in such conditions, and the engine would be near the limit of the working range as the inlet temperature is just 275.2 K. The current design of the engine room is not suited to Arctic conditions, and improvements should be made, such as pre-heating the air before it enters the room, or reducing the flow into the room. The hot air of the Genset outlet could be utilised further by using ducting to mix it with the incoming air, rather than expending further energy by using electrical preheaters. Other areas within the engine room where energy could be extracted include the high temperature exhausts which are currently directed out of the room by lagged pipes. A heat exchanger could be implemented to heat the air as it enters the room. The effectiveness of heat removal for the Case 2 was 0.99.

The temperature distribution for the tropics, Case 3, shows the smallest range. This is to be expected, as the inlet temperature is only 25.0 K below the Genset outlet temperature. The same trend is present as the other cases, but it is much less noticeable, with all data point locations within 310.0 – 320.0 K. The British Standard states that a marine vessel engine room's ventilation system should ensure that the temperature rise from inlet to entrance of the engine room should not exceed 12.5 K when the intake temperature is 308.0 K. The entrance to the engine room is adjacent to the outlet, and has a temperature of 319.9 K which means that the current design of the engine room complies with standard, as the temperature rise is 11.9 K. The effectiveness of heat removal for the Case 3 was 0.99.

The heat removal effectiveness for the three cases was remarkably similar; Case 1, $\varepsilon_T = 0.98$, Case 2 $\varepsilon_T = 0.98$, and Case 3, $\varepsilon_T = 0.99$.

### *7.3. Ducted studies*

#### *7.3.1. Ducted inlet study*

By changing the inlet conditions to the engine room, the thermal profile of the room changes considerably from the baseline case, Case 1. The temperature data sets at the data locations are shown in Fig. 11, and contour plots for a plane along the *x*-axis in Fig. 12, the heat removal effectiveness is shown in Table 4.

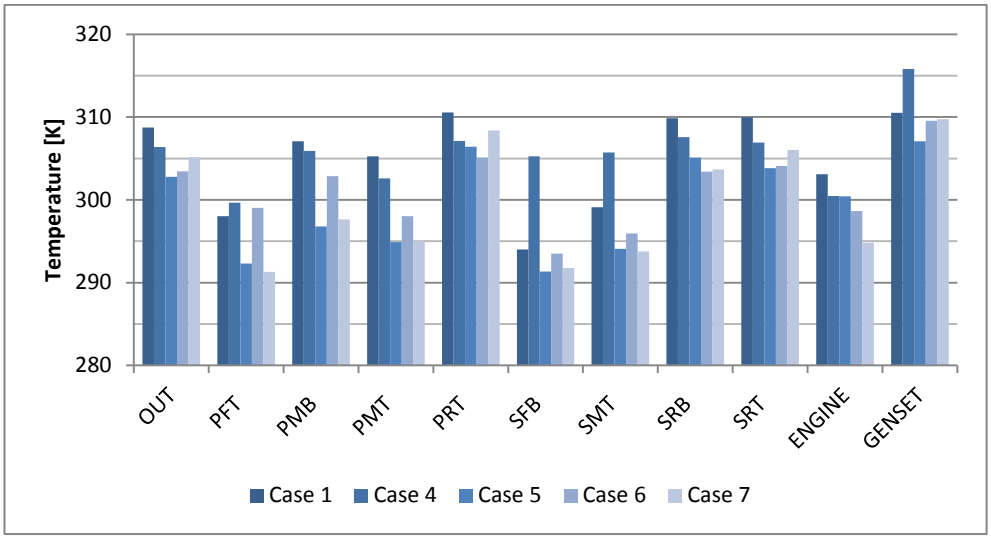


**Fig. 11.** Temperature at data locations for ducted inlet study. The inlets switched on for each case were: Case 1 – Inlet, Case 4 – mid_E and mid_G, Case 5 – Inlet and mid_E, Case 6 – Inlet and mid_G, Case 7 – Inlet, mid_E and mid_G.

**Table 4.** Heat removal effectiveness for ducted inlet study

| Name | Inlets on | $\varepsilon_T$ |
|---|---|---|
| Case 1 | Inlet | 0.98 |
| Case 4 | midE, midG | 1.04 |
| Case 5 | Inlet, midE | 0.98 |
| Case 6 | Inlet, midG | 1.00 |
| Case 7 | Inlet, midE, mid G | 0.99 |

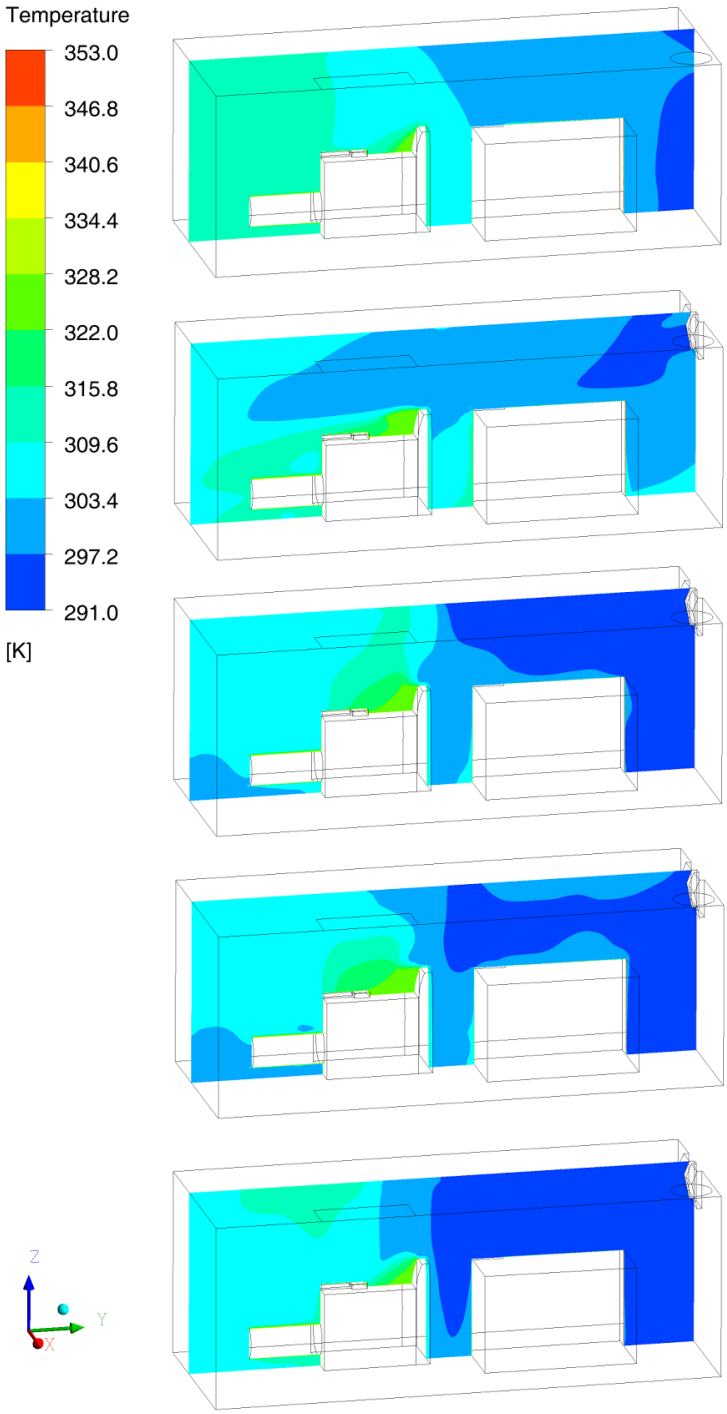


**Fig. 12.** Temperature profiles of engine room for ducted inlet study (*yz* plane at $x = 0.705$ m); from top to bottom, cases and inlets: Case 1 (Inlet), Case 4 (mid_E and mid_G), Case 5 (Inlet and mid_E), Case 6 (Inlet and mid_G), Case 7 (Inlet, mid_E and mid_G).

In Case 4 the main inlet is not used, but only the mid_E and mid_G inlets; the thermal profile of the room generally increases in temperature at the data points, most noticeably on the starboard side of the room, and towards the front. This is due to the inlets being positioned towards the port side of room. The only benefit of this configuration is the engine intake temperature is slightly reduced, which promotes better use of fuel and increased efficiency, however, in contrast, the Genset intake temperature is increased drastically.

All other combinations of inlets reduce the temperature at data points, apart from Case 6, where PFT increases by 1.0 K. The combination of the inlets working together ensures that the flow does not channel down the starboard side, and reaches all corners of the room, including SRT which is situated to the rear of the outlet.

The heat removal effectiveness is similar for all the cases, with the best performing being Case 4, and both Case 1 and Case 5 joint worst. However, the most important part of the thermal profile is the engine intake temperature; if the temperature is reduced, the efficiency of the engine can be increased. The engine will be able to produce more power for the same amount of fuel due to the combustion of the fuel with the increased density of air. Fig. 13 shows the changes from rated power of the engine and Genset due to the intake temperatures.

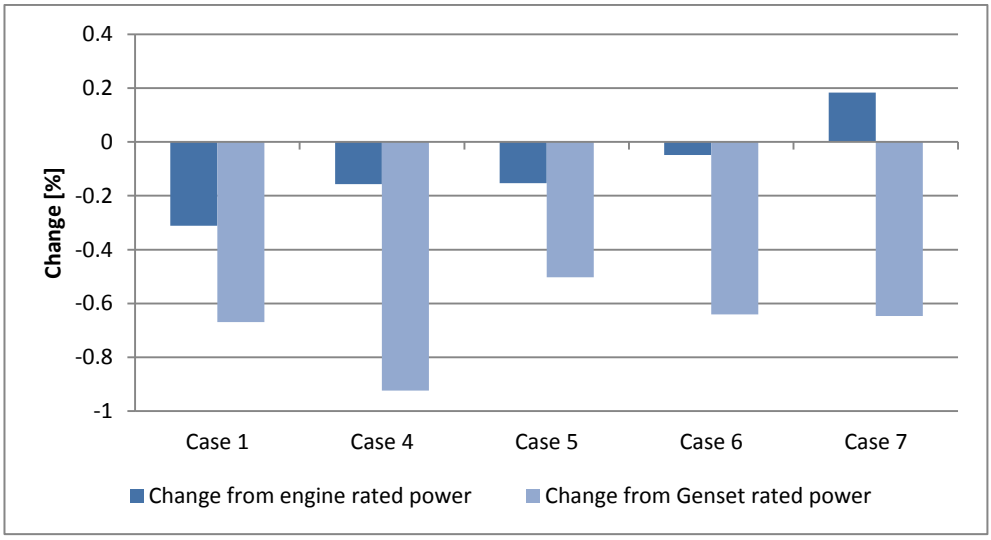


**Fig. 13.** Change from engine and Genset rated power for ducted inlet study. The inlets switched on for each case were: Case 1 – Inlet, Case 4 – mid_E and mid_G, Case 5 – Inlet and mid_E, Case 6 – Inlet and mid_G, Case 7 – Inlet, mid_E and mid_G.

The changes from rated power for the engine are improved for all new layouts, whilst for the Genset, Case 4 is worse, going from -0.67 % to -0.92 %. Although the Genset power has decreased, the engine has increased from -0.31 % to -0.16 %, and in terms of energy and cost, the engine is most important, as it will run for much longer periods compared to the Genset, and use much more fuel. The greatest improvement is found for Case 7, where there is an increase from rated power of 0.18 %.

*7.3.2. Ducted Genset outlet study*

In general, all cases have shown that the rear of the engine room has the hottest region; this is due to the Genset outlet pumping hot air into the rear vicinity. The following cases show a very different thermal profile, due to the Genset outlet boundary condition being turned off to represent the hot air being ducted directly out of the room. Fig. 14 shows the temperatures at the data point locations, and Fig. 15 shows the corresponding contour plots. The heat removal effectiveness is shown in Table 5.

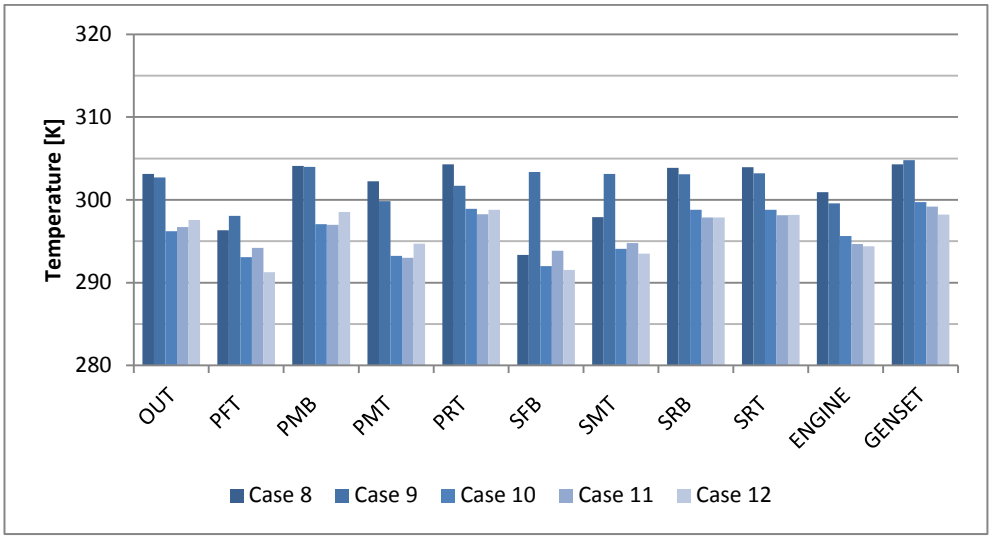


**Fig. 14.** Temperature at data locations for ducted Genset outlet study. The inlets switched on for each case were: Case 8 – Inlet, Case 9 – mid_E and mid_G, Case 10 – Inlet and mid_E, Case 11 – Inlet and mid_G, Case 12 – Inlet, mid_E and mid_G.

**Table 5.** Heat removal effectiveness for ducted genset outlet study

| Name | Inlets on | $\varepsilon_T$ |
|---|---|---|
| Case 8 | Inlet | 0.99 |
| Case 9 | midE, midG | 1.04 |
| Case 10 | Inlet, midE | 0.75 |
| Case 1 | Inlet, midG | 0.90 |
| Case 12 | Inlet, midE, mid G | 1.03 |

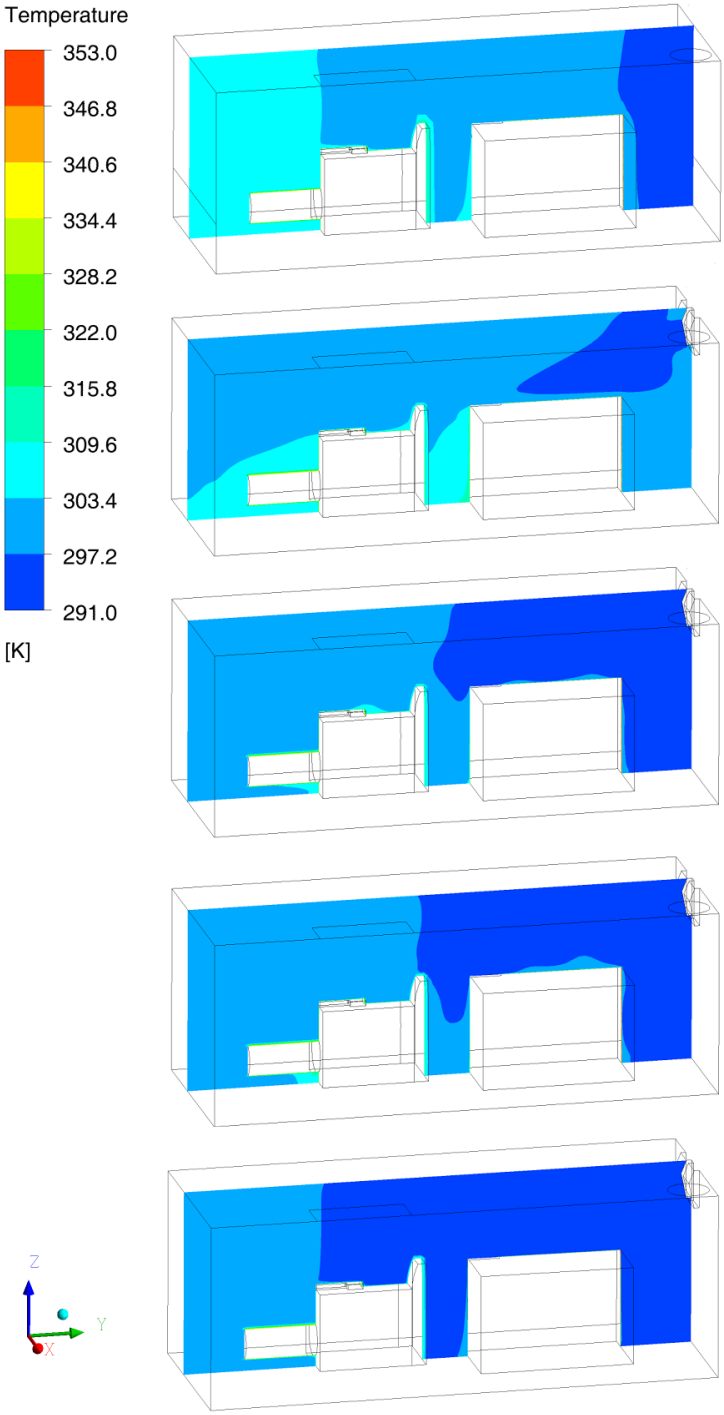


**Fig. 15.** Temperature profiles of engine room for ducted Genset outlet study (*yz* plane at $x = 0.705$ m); from top to bottom, cases and inlets: Case 8 (Inlet), Case 9 (mid_E and mid_G), Case 10 (Inlet and mid_E), Case 11 (Inlet and mid_G), Case 12. (Inlet, mid_E and mid_G).

The temperatures at the data point locations for all cases are below 305.0 K. Fig. 12 and Fig. 15 present different temperature contours due to the Genset not adding heat into the room; the ranges have decreased for all cases. The front and middle starboard side of Case 9 shows the same trend as Case 4, where the temperatures are higher than that of the baseline case, or in this instance, when the Genset outlet boundary conditions has been turned off, Case 8. Overall, the temperature profile for the mixed inlets cases is lower again. The temperatures for

the Genset inlet are lower for all cases. The heat removal effectiveness has improved for Case 8 and 12, however, has dropped dramatically for Case 10. Although the mean temperature is lower in the room, the flow profile has changed due to the Genset outlet being turned off. The changes from rated power are shown in Fig. 16.

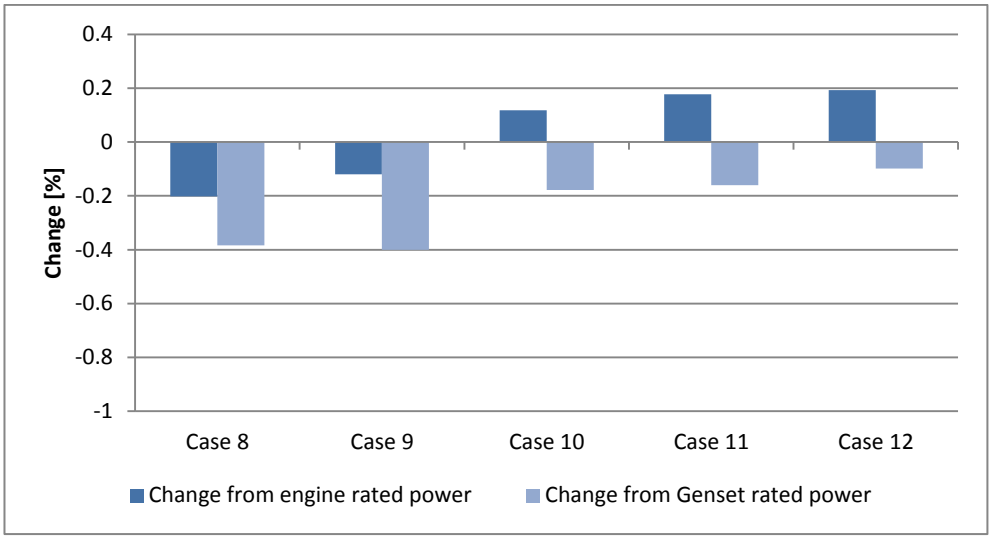


**Fig. 16.** Change from engine and Genset rated power for ducted Genset outlet study. The inlets switched on for each case were: Case 8 – Inlet, Case 9 – mid_E and mid_G, Case 10 – Inlet and mid_E, Case 11 – Inlet and mid_G, Case 12 – Inlet, mid_E and mid_G.

Whilst the heat removal effectiveness was lower for Case 10, there were improvements for the change in rated power for both the engine and genset. Due to the intake temperatures for the Genset, the change from rated power has reduced for all cases. The same is true for the engine, where the change in rated power has been improved for all cases. Cases 10 – 12 improve on the standard reference power, with Case 12 outperforming the rest with a change from rated power of 0.2 %.

## 8. Conclusions

A marine vessel engine room has been modelled using CFD. Experimentation on the actual marine vessel engine room provided boundary conditions and data to validate the model. It has been shown that the model is in good agreement with the data from the experimental work.

The model has been used to investigate how the marine vessel would cope with extreme climates such as the Arctic or tropical seas. With the current configuration, the marine vessel engine room would not provide a comfortable working temperature for Arctic temperatures, and the overall temperature within the room would need to be increased by adding heat to the incoming air, or by reducing the flow into the room. The current ventilation system would satisfy the British Standard for ventilation in tropical waters, with the heat addition from inlet to entrance to the engine room being within the limit imposed by the standard.

Ducting the inlet to direct flow around the room has shown an improvement in overall thermal profiles and specifically in terms of engine and Genset intake temperatures. The decreased temperature of the air results in higher air density at the engine and Genset intakes, thus achieving a leaner combustion which yields higher efficiencies.

By ducting the Genset outlet directly out of the room, and dividing the flow into three inlets across the front top of the engine room, an increase in engine and Genset power of 0.5 % and 0.57 % respectively is achieved for the same fuel rates from the current ventilation system.

Whilst these are relatively modest increases, which result in an overall efficiency improvement of 0.2 % from the rated power for the engine, over the lifetime of the marine vessel, substantial savings in fuel and energy can be made. The impact of these efficiencies could be examined in the future by undertaking a life cycle analysis.

## Acknowledgements

The authors would like to acknowledge the support of the Advanced Sustainable Manufacturing Technologies (ASTUTE) project, which is part funded from the EU's European Regional Development Fund through the Welsh European Funding Office, in enabling the research upon which this paper is based. Further information on ASTUTE can be found at www.astutewales.com

## References

[1] BS EN ISO 8861:1998, "Shipbuilding - Engine-room ventilation in diesel-engined ships - Design requirements and basis of calculations," *British Standards*, 1998.

[2] P. Mustakallio and R. Kosonen. (2014) AIHIA. [Online]. https://www.aiha.org/aihce06/handouts/b2mustakallio.pdf

[3] Caterpillar, "Engine Room Ventilation," 2008.

[4] Cummins Fire Power. (2009) Engine Room Ventilation Calculations. [Online]. www.cumminsfirepower.com/documents/ES027_ventilation.pdf

[5] P. Rohdin and B. Moshfegh, "Numerical modelling of industrial indoor environments: A comparison between different turbulence models and supply systems supported by field measurements," *Building and Environment*, vol. 46, pp. 2365 - 2374, 2011.

[6] J. D. Posner, C. R. Buchanan, and D. Dunn-Rankin, "Measurement and prediction of indoor air flow in a model room," *Energy and Building*, vol. 35, pp. 515 - 526, 2003.

[7] T. Zhang, P. Li, and S. Wang, "A personal air distribution system with air terminals embedded in chair armrests on commercial airplanes," *Building and Environment*, vol. 47, pp. 89-99, 2012.

[8] B. S. Aranjo, B. R. Hughes, and H. N. Chaudry, "Performance investigation of ground cooling for the airbus A380 in the United Arab Emirates," *Applied Thermal Engineering*, vol. 36, pp. 87-95, 2012.

[9] I. Bayraktar, "Computational simulation methods for vehicle thermal management," *Applied Thermal Engineering*, vol. 36, pp. 325-329, 2012.

[10] J. C. Ramos et al., "Numerical modelling of the natural ventilation of underground transformer substations," *Applied Thermal Engineering*, vol. 51, no. 2013, pp. 852-863, 2013.

[11] V. Yakhot and S. A. Orszag, "Renormalization group analysis of turbulence," *Journal of Scientific Computing*, vol. 1, no. 1, pp. 3-51, 1986.

[12] ANSYS FLUENT Theory Guide (Accessed 2013). [Online]. www.ansys.com

[13] T.-H. Shih, W. W. Liou, A. Shabbir, Z. Yang, and J. Zhu, "A new k-ϵ eddy viscosity model for high reynolds number tubulent flows," *Computers & Fluids*,

vol. 24, no. 3, pp. 227-238, 1995.

[14] Z. Zhai, Z. Zhang, W. Zhang, and Q. Chen, "Evaluation of Various Turbulence Models in Predicting Airflow and Turbulence in Enclosed Environments by CFD: Part-1: Summary of Prevalent Turbulence Models," *HVAC&R Research*, vol. 13, no. 6, 2007.

[15] ANSYS ICEM CFD User Manual (Accessed 2012). [Online]. www.ansys.com

[16] Suhas V. Patankar, *Numerical Heat Transfer and Fluid Flow*, 1st ed.: Taylor & Francis, 1980.

[17] H. Awabi, *Ventilation of buildings*.: Taylor and Francis, 2003.

[18] BS ISO15550:2002, "Internal combustion engines - Determination and method for the measurement of engine power - General requirements," *British Standards*, 2002.

[19] W. Oberkampf and T. Trucano, "Verification and validation in computational fluid dynamics," *Progress in Aerospace Sciences*, vol. 38, pp. 209-272, 2002.